Renewable and Sustainable Energy Reviews 151 (2021) 111533

Contents lists available at ScienceDirect

Renewable and Sustainable Energy Reviews

journal homepage: www.elsevier.com/locate/rser

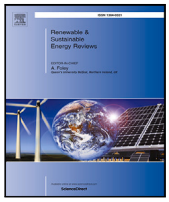

Sequential steady-state security region-based transmission power system resilience enhancement

Chong Wang [a,*], Ping Ju [a], Feng Wu [a], Shunbo Lei [b], Xueping Pan [a]

[a] College of Energy and Electrical Engineering, Hohai University, Nanjing 211100, China
[b] Department of Electrical Engineering and Computer Science, University of Michigan, Ann Arbor, MI, 48109, USA

ARTICLE INFO

Keywords:
Resilience
Bi-level programming model
Power system
Sequential steady-state security region
System topology

ABSTRACT

The increased high-impact and low-probability extreme weather events have posed unprecedented impacts on power system operation, and it is necessary to have appropriate methods to analyze the impacts. In this paper, a sequential steady-state security region (SSSR) is proposed to better describe the operational region impacted by sequential weather events, and SSSR is a polytope describing a region, where the operational constraints are satisfied. Based on SSSR with uncertain topology changes because of extreme weather events, a bi-level programming model is proposed. By means of Karush–Kuhn–Tucker conditions, the lower-level optimization model is equivalently transformed into a set of linear constraints, which are included in the upper-level optimization model. System topology scenarios are generated with the Monte Carlo method to avoid the curse of dimensionality caused by numerous uncertain topology scenarios. The generated system topology scenarios are mapped into the binary variables, representing line states, by means of the recursive McCormick (RMC) envelopes. Two test systems validate the proposed model. The results show that the proposed SSSR can well describe the feasible sequential region with regard to extreme weather events.

1. Introduction

Energy has played a critical role in supporting social development. In Asia and the Pacific, the primary energy demand is estimated to have more than 2.4% increase each year by 2030, typically electricity demand has a higher increase, at about 3.4%. For the increased electricity demand, it is desired to have efficient and reliable power supply. The power systems usually cover wide geographical regions, and many of components in the power systems are exposed to external environment, which makes the power systems vulnerable to natural disasters, e.g., wind storms, ice storms, thunderstorms, earthquake, fires, and flooding [1–3]. The global temperature rise has been considered as one of important underlying causes of the extreme weather events with the higher intensity and frequency [4,5]. Based on the data reported to the Department of Energy of U.S. from 2000 to 2016, including outages due to extreme weather events, equipment failure, operation disruption, fuel supply emergency, system islanding, intentional attacks, and public appeal, it is observed that weather-related major power outages account for 52.9% of total power outages [6]. For example, Hurricane Sandy in 2012 had a severe impact on the power supply system of New York. Flooding caused by Sandy made five important transmission substations shut down, and one third of generation was lost, affecting more than two million residents. In addition, 1000 poles and 225 miles of overhead lines in the distribution systems were damaged due to the high wind speed, reaching the maximum speed of 145 kilometers per hour [7]. On 23 June 2015, more than 280,000 residents were affected by a storm, with the similar intensity of Hurricane Sandy, and more than 250,000 people in Philadelphia were affected at the same time [8]. In 2011, two high-voltage transmission lines in New Mexico were threatened by the Las Conchas wildfire, resulting in 400,000 customers at risk, and Los Alamos National Laboratory was also forced to be closed due to this fire [8]. In September 2015, an extreme high temperature in San Diego resulted in load shedding to guarantee power balance, and about 150 MW loads were curtailed with 115,000 customers in blackout [8]. Another recent weather-related outage was Texas power outage in February 2021. A rare polar vortex caused 50 °F below average temperature in Texas, resulting in more than 69 GW of loads at the peak. In addition, the severe cold air forced some wind turbines and natural gas facilities out of service [9]. In Texas, the electricity produced by natural gas in 2020 and wind in 2017 was more than 50% and 15% [10,11], respectively. The rare polar vortex caused five million people at the peak without power.

* Corresponding author.
E-mail addresses: chongwang@hhu.edu.cn (C. Wang), pju@hhu.edu.cn (P. Ju), wufeng@hhu.edu.cn (F. Wu), shunbol@umich.edu (S. Lei), xueping_pan@hhu.edu.cn (X. Pan).

https://doi.org/10.1016/j.rser.2021.111533
Received 6 January 2021; Received in revised form 26 April 2021; Accepted 24 July 2021
Available online 11 August 2021
1364-0321/

Nomenclature

Sets and Indices

b', b	Index representing buses.
t	Index representing time periods.
k	Index representing scenarios of sequential system topologies.
g	Index representing generating units.
l	Index representing lines.
$\bar{\mathcal{L}}$	Set of lines, which will not be on the trajectory of an unfolding event.
$\mathcal{B}_b$	Set of buses that are connected to bus b.
$\mathcal{L}$	Set of lines, which will be on the trajectory of an unfolding event.
$\mathcal{G}_b$	Set of generators that are connected to bus b.
Ψ_1, Ψ_2, Ψ_K	Different sequential steady-state security regions.
Π_k	Sequential system topology under the kth scenario.
Ω	Set of all possible SSSRs.

Parameters

N	The number of time intervals.
$B_{bb'}$	Electrical susceptance.
$\mathbf{a}, \mathcal{A}, \mathbf{b}, \mathcal{B}, C$	Coefficient matrices.
$\underline{R}_g, \overline{R}_g$	Ramp-down and ramp-up limits of generators.
$\overline{P}_{bt}$	Bus load.
$\overline{P}_{bb'}$	The capacity of line $b-b'$.
$\underline{P}_g, \overline{P}_g$	Generation bounds.
$\underline{\theta}_b, \overline{\theta}_b$	Voltage angle limits of bus b.

Variables

P_{gt}	Active power at t.
$P_{bb'tk}$	Power flow of line $b-b'$ at t regarding the sequential topology scenario Π_k.
θ_{btk}	Bus angle at t under the sequential topology scenario Π_k.
f, F	Optimization objectives.
$u_{bb'tk}$	Binary variable representing the on–off state of the line $b-b'$ at time t regarding the sequential topology scenario Π_k. '1' and '0' indicate on-state and off-state, respectively.
$(\mathbf{s}^+)^*, (\mathbf{s}^-)^*$	Vectors of optimal slack variables for the lower level model.
$\mathbf{s}^+, \mathbf{s}^-$	Positive slack variable vectors.
L_F	Lagrangian function.
$\mathcal{U}$	Vector of binary variables that represent system topologies.
$\mathcal{Y}^*$	Vector of optimal continuous variables of the second level model.
$\mathcal{Y}$	Vector of continuous variables that represent system conditions.
$\alpha, \gamma, \beta,$	Vectors of Lagrange multipliers, respectively.
$\hat{\alpha}, \hat{\beta}, \hat{\gamma}$	Diagonal matrices of Lagrange multipliers corresponding to α, β, γ, respectively.

The increased extreme weather events and the corresponding power outages have driven the governments and the international organizations, the North American Electric Reliability Corporation (NERC), the United States Electric Power Research Institute (EPRI), and the House of Lords in the United Kingdom , focus their attentions on power system resilience [12–14]. The National Infrastructure Advisory Council in October 2010 released a report that presents a resilience structure with four features, shown in Fig. 1, based on the sequence of "prior to events", "during events", "after events", and "post-incident learning", respectively [15–17]. Prior to events, "robustness" requires to stay standing or keep operating in the face of extreme weather events. Sometimes, strengthening the system is one of acceptable preventive strategies. Furthermore, maintaining and investing in elements of critical infrastructure could also improve system robustness so that they can withstand these extreme weather events. During events, "resourcefulness" requires to have enough capability of managing an event as it unfolds. In this stage, it is necessary to identify options and prioritize what could be done to mitigate the caused damages. After events, it is desired to get the system back to normal states as quickly as possible. To this end, determining emergency and restoration operations is important, and scheduling the appropriate sources and the right people to the right place is also critical [18,19].

The conventional operational strategies usually do not include the countermeasures against these potential extreme weather events. It is crucial to make appropriate strategies to deal with these extreme weather events. To cover the whole time horizon of an extreme weather event, the strategies in different stages, i.e., prior to the event, during the event, and after the event, should be prepared [20–22].

Prior to the event, assessments and preventive strategies need to be implemented to improve the system capability of dealing with an extreme weather event. A historical data-based regression model is established to evaluate the potential outages due to hurricanes [23]. In addition to hurricanes, the influences of extreme floods and wildfires on power systems are investigated in [24,25]. Power system resilience assessments on transmission and distribution systems are investigated in [26]. Based on the assessments, potential preventive countermeasures, e.g., microgrid construction, mobile energy storage pre-allocation, and network hardening, can be implemented to increase the system resilience [27,28]. For example, preventive resource allocation in consideration of repair and restoration for possible failures on the trajectory of one upcoming hurricane is investigated in [29]. To minimize the number of vulnerable lines impacted by an approaching hurricane, the optimal microgrid formation is analyzed in [30]. A tri-level optimization model is proposed in [31] to construct optimal hardening strategies, improving distribution system resilience. In consideration of the flexibility of mobile power sources, [32] focuses on optimal pre-position for mobile power sources to make critical loads have high survivability after outages. [33] investigates a resilience-oriented proactive strategy to improve the preparedness of multiple microgrids against one upcoming hurricane.

During the event, real-time strategies are expected to be performed to mitigate the negative impacts. [34] proposes a microgrid sectionalization approach to enhance distribution system resilience, and an operational enhancement method based on a defensive islanding algorithm is proposed in [35], and the potential cascading failures can be avoid. Real-time strategies, including topology switching, load shedding, and generation dispatch, associated with preventive strategies are presented in [36] to construct an integrated resilience response framework. Considering the forced outages of lines and heterogeneity of power flow distribution, a resilience-constrained unit commitment model is established in [37]. Resilience enhancement strategies, during an unfolding extreme event, based on Markov decision processes are

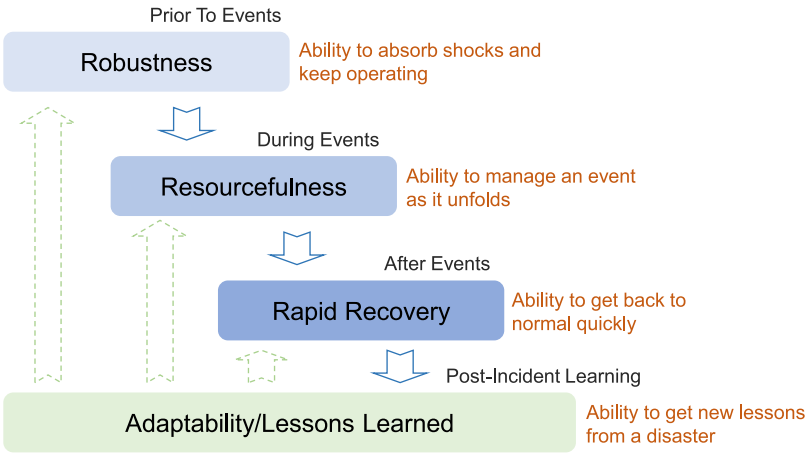

Fig. 1. Resilience structure.

proposed in [38,39]. Based on Markov states, a recursive optimization model in consideration of the future expected cost and the current cost is established, and the real-time states can be mapped into the optimal strategy in each decision period.

After the event, it is necessary to quickly restore the system. Constructing microgrids is an effective means to quickly pick up loads after a disaster [40]. An approach to restore critical loads by constructing multiple microgrids, in which there are distributed generators, is investigated in [41]. A load restoration architecture is proposed in [42] to enhance the feeder-level resilience in distribution systems. Repair crews and mobile power sources play important roles in load restoration after disasters. [43] dispatches mobile power sources and repair crews to restore the distribution system, and the problem is constructed as a mixed integer linear programming model.

Currently, many of research studies focus on microgrid construction, repair crew dispatch, system hardening, and mobile emergency resource dispatch to improve the resilience of distribution power systems. In consideration of different characteristics between transmission systems and distribution systems, the effects of these strategies are restricted for transmission systems. When a transmission system is being impacted by an extreme weather event, how to consider uncertain sequential impacts on the system and depict the corresponding feasible region in consideration of the operational constraints to improve power system resilience is one of significant research points that need to be further investigated. To bridge a gap in this point, a sequential steady-state security region (SSSR) is proposed in this paper to better describe the operational region impacted by sequential weather events, and a SSSR-based system optimization model to determine an operational point to improve system resilience is investigated. There are three main contributions listed as follows: (1) A sequential steady-state security region is proposed to describe the operational region impacted by the sequential weather event; (2) The SSSR-based resilience enhancement problem in consideration of uncertain system topology changes caused by the extreme weather event is established as a bi-level programming model; (3) The sequential system topology changes are mapped into new optimization variables associated with a set of constraints by using recursive McCormick envelopes.

2. Sequential steady-state security region in consideration of event uncertainty

2.1. Sequential steady-state security region

Different lines on the trajectory of an unfolding event may be in failure during the sequential time periods of the event, and in consequence can lead to different topologies during its sequential time periods. For example, $\{b_{12}, b_{14}\}$ and $\{b_{14}, b_{16}\}$ are the sets of potential failure components in t_1 and t_2 in Fig. 2, respectively. Because of the uncertain influences of the unfolding event on the network, there are different possible failure scenarios. For example, the failure scenario may be $\{b_{14}\}$ and $\{b_{14}, b_{16}\}$ in t_1 and t_2, respectively. It means that the line b_{14} is in failure in t_1 and the lines b_{14} and b_{16} are in failure in t_2. For another example, the failure scenario may be $\{\emptyset\}$ and $\{b_{14}\}$ in t_1 and t_2, respectively. It means that no line is in failure in t_1 and the line b_{14} is in failure in t_2. Feasible operational points over the sequential time periods are expected for possible failure scenarios that are bounded by the operational constraints such as line capacity, generators' ramping rates and generator capacity. Therefore, appropriate operational points play significant roles in the subsequent operational points over the sequential time periods. To illustrate the importance of the operational points, the steady-state security region (SSR) [44] is introduced.

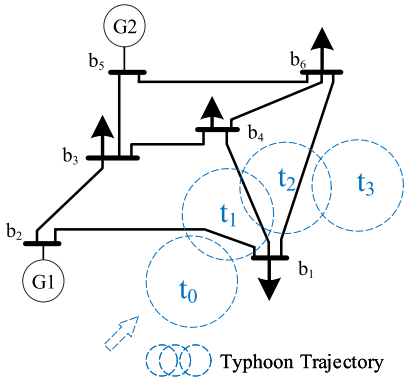

Fig. 2. Sequential impacts caused by an unfolding event.

For the SSR, the operational constraints are the space boundaries, and it is usually constructed to deal with the problem with one time period. An operational point can be easily checked if it is steady-state secure based on SSR. For example, there are two generators in Fig. 3. At t_0, the operational points o_1, o_4, and o_6 are within SSR, and they are steady-state secure. However, when we consider the sequential time periods of an event, the corresponding SSR will be complicated.

For example, the operational point o_1 in t_1 can reach the operational point o_2 in t_2, and then can reach the operational point o_3 in t_3 with the constraints of generators' ramping rates. However, the operational point o_4 can only reach the purple rectangular region, which is not within SSR in t_2. Similarly, the operational point o_7 can only reach the purple rectangular region, which is not within SSR in t_3. Therefore, based on SSR, the concept of a sequential steady-state security region (SSSR) is proposed in consideration of the sequential impacts.

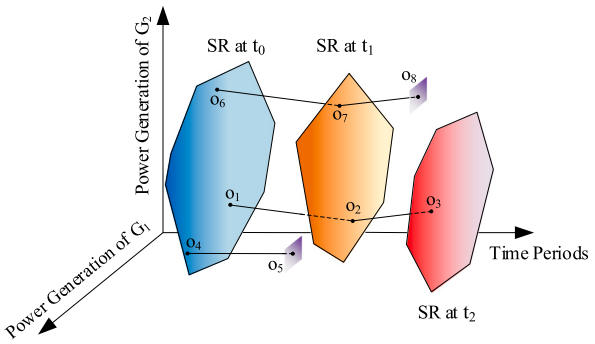

Fig. 3. Security region (SR) over sequential time periods.

The generic mathematical expression for SSR is written as (1).

$$\psi\{\mathbf{y}|\mathbf{a}\cdot\mathbf{y}\le\mathbf{b}\} \tag{1}$$

where $\mathbf{a}$ is a coefficient matrix and $\mathbf{b}$ is a coefficient vector representing operating constraints, and $\mathbf{y}$ is a vector of variables, representing generators' outputs. The constraint (1) represents the steady-state security region of one time interval. Considering the sequential time periods, the constraint (1) can be extended to SSSR, which can be represented as follows.

$$\mathcal{Y}=[\mathbf{y}_1^T,\dots,\mathbf{y}_t^T\cdots,\mathbf{y}_N^T]^T \tag{2a}$$

$$\mathcal{B}=[\mathbf{b}_1^T,\dots,\mathbf{b}_t^T\cdots,\mathbf{b}_N^T]^T \tag{2b}$$

$$\mathcal{A}=\begin{bmatrix} a_1 & a_{12} & & & & \\ a_{21} & a_2 & a_{23} & & & \\ & a_{32} & a_3 & & & \\ & & & \ddots & & \\ & & & & a_{N-1} & a_{N-1,N} \\ & & & & a_{N,N-1} & a_N \end{bmatrix} \tag{2c}$$

$$\Psi\{\mathcal{Y}|\mathcal{A}\cdot\mathcal{Y}\le\mathcal{B}\} \tag{2d}$$

where $\mathcal{A}$ is a coefficient matrix extended from $\mathbf{a}$, and $\mathcal{B}$ is a coefficient vector extended from $\mathbf{b}$ in consideration of different time periods. $\mathcal{Y}$ is a variable vector that is extended from $\mathbf{y}$ in consideration of different time periods. The subscripts $1,\dots,t,\dots,N$ denote different time intervals. $\mathcal{A}$ is a sparse matrix, in which the diagonal submatrices $a_1,a_2,\dots,a_N$ denote the coefficient with regard to operational constraints in the $1\text{st},2\text{nd},\dots,T\text{st}$ time periods. $\mathbf{a}_{12}$ and $\mathbf{a}_{21}$ show the coupling relations in the 1st and 2nd time periods. $\mathbf{a}_{23}$ and $\mathbf{a}_{32}$ show the coupling relations in the 2nd and 3rd time periods. The coupling relations are determined by the generators' ramping rates, and the other elements in the matrix $\mathcal{A}$ are zeros.

2.2. SSSR with uncertain system topology changes

SSSR can describe the sequential characteristics over the sequential time periods. In consideration of uncertain influences of an unfolding event on the topology, it is necessary to include these uncertainties in SSSR. Fig. 4 shows an example. To read the figure easily, the 3-dimension figure is illustrated by several 2-dimension figures. The steady-state security regions in t_0, t_1, and t_2 are illustrated in Fig. 4(a), (b), and (c), respectively. Even though the probabilities of line failures due to the unfolding event are assumed to be known, the system topologies in the subsequent periods t_1 and t_2 cannot be known due to uncertain line failures in t_1 and t_2 when determining the strategy in t_0. This results in different possible SSSRs. Therefore, it is desired to obtain strategies that are within the feasible regions in t_1 and t_2 considering possible SSSRs. A new set Ω, representing all possible SSSRs, is defined as follows.

$$\Omega=\{\Pi_1,\Pi_2,\dots,\Pi_K\}$$

where Π_1, Π_2, and Π_K are different SSSRs corresponding to different sequential system topologies $\Pi_1=\{\pi_{11},\dots,\pi_{1N}\}$, $\Pi_2=\{\pi_{21},\dots,\pi_{2N}\}$, and $\Pi_K=\{\pi_{K1},\dots,\pi_{KN}\}$. π_{KN} is a system topology scenario of the Kth SSSR in time N.

Currently, many research studies focus on the information of typhoons [45], and furthermore the weather-related information can be known from the meteorological departments to obtain typhoon information with its trajectory and its corresponding speed. When a power system is impacted by a typhoon, the component failure is usually caused by the high wind speed. The component failure probabilities with regard to wind speeds have been investigated in many existing studies [46]. Therefore, it is assumed that the trajectory of the typhoon and the component failure probabilities are known in the study.

3. Resilience enhancement based on bi-level programming model

Considering uncertain system topology changes, the mathematical formulation of SSSR is first presented, and then the bi-level programming model based on the mathematical formulation of SSSR for resilience enhancement is established.

3.1. Mathematical formulation of SSSR

For the sequential system topology Π_k caused by an extreme weather event, we can express its corresponding mathematical SSSR as follows.

$$\sum_{g\in G_b}P_{gt}-P_{bt}+\sum_{b'\in B_b}P_{bb't}=0\quad\forall t,b \tag{3a}$$

$$B_{bb'}(\theta_{bt}-\theta_{b't})=P_{bb't}\quad\forall t,(b,b')\in\Pi_K \tag{3b}$$

$$\underline{P}_g\le P_{gt}\le\overline{P}_g\quad\forall g,t \tag{3c}$$

$$\underline{R}_g\le P_{g(t+1)}-P_{gt}\le\overline{R}_g\quad\forall g,t \tag{3d}$$

$$\underline{P}_{bb'}\le P_{bb't}\le\overline{P}_{bb'}\quad\forall t,(b,b')\in\Pi_K \tag{3e}$$

where (3a) presents the power balance constraint, (3b) shows the linear simplification of line power flow with regard to voltage angles, (3c) presents the lower/upper bounds of generators' outputs, (3d) presents the constraint of the generators' ramping rates, and (3e) shows the line capacity bounds.

Based on (3), its corresponding generic expression can be represented as follows.

$$\exists\mathcal{Y}:\ \mathcal{A}\cdot\mathcal{Y}\le\mathcal{B} \tag{4}$$

The generic constraint (4) means that there exists a strategy, satisfying the operational constraints, over the sequential time periods under a given SSSR. To obtain this strategy, two new positive slack vectors $\mathbf{s}^+$ and $\mathbf{s}^-$ are introduced into the model, and a new optimization model can be constructed.

$$f(\mathcal{Y})=\min_{\mathbf{s}^-,\mathbf{s}^+,\mathcal{Y}}\ \mathbf{1}^T\mathbf{s}^-+\mathbf{1}^T\mathbf{s}^+ \tag{5a}$$

$$s.t.\ \ \mathbf{s}^+\ge\mathbf{0},\quad\mathbf{s}^-\ge\mathbf{0} \tag{5b}$$

$$\mathbf{s}^+-\mathbf{s}^-+\mathcal{A}\cdot\mathcal{Y}\le\mathcal{B} \tag{5c}$$

where $\mathbf{1}$ is a vector including 1 with proper dimensions, and $\mathbf{0}$ is a vector including 0 with proper dimensions. If we have $f(\mathcal{Y})=0$, it is concluded that $\mathcal{Y}\neq\emptyset$ holds. When we have $f(\mathcal{Y})>0$, it means there is no strategy satisfying the operational constraints, i.e., $\mathcal{Y}=\emptyset$.

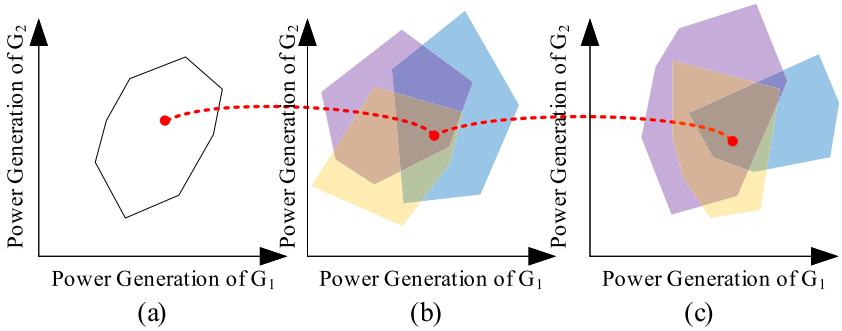

Fig. 4. Sequential steady-state security region (SSSR) illustrated by the 2-dimension figures.

3.2. SSSR in consideration of uncertain system topology changes

Because of the uncertain impacts caused by the event on the system, the system topology on the event trajectory is uncertain. Considering possible system topology changes, SSSR can be represented as follows.

$$\sum_{g\in G_b} P_{gt} - P_{bt} + \sum_{b'\in B_b} P_{bb'tk} = 0 \quad \forall t,b,k \tag{6a}$$

$$B_{bb'}(\theta_{btk} - \theta_{b'tk}) = P_{bb'tk} \quad \forall t,(b,b') \in \Pi_k, k \tag{6b}$$

$$\underline{P}_{bb'} \le P_{bb'tk} \le \overline{P}_{bb'} \quad \forall k,t,(b,b') \in \Pi_k \tag{6c}$$

$$\underline{R}_g \le P_{g(t+1)} - P_{gt} \le \overline{R}_g \quad \forall t,g \tag{6d}$$

$$\underline{P}_g \le P_{gt} \le \overline{P}_g \quad \forall t,g \tag{6e}$$

$$\underline{\theta}_b \le \theta_{btk} \le \overline{\theta}_b \quad \forall t,b,k \tag{6f}$$

where the subscript k in (6a)–(6f) represents the possible topology scenarios due to the unfolding event, and in consequence (6a)–(6f) have direct relations to the system topologies. However, (6a)–(6f) cannot be directly optimized as the constraints because of their non-explicit characteristics with regard to the optimization variables, i.e., generator outputs and line states. To relate the system topologies to the optimization variables, the constraints are rewritten by introducing integer variables representing on–off line states.

$$\sum_{g\in G_b} P_{gt} - P_{bt} + \sum_{b'\in B_b} P_{bb'tk} = 0 \quad \forall t,b,k \tag{7a}$$

$$B_{bb'}(\theta_{btk} - \theta_{b'tk}) - P_{bb'tk} + (1-u_{bb'tk})M \ge 0 \quad \forall l \in \mathcal{L}, t,(b,b') \in l \tag{7b}$$

$$B_{bb'}(\theta_{btk} - \theta_{b'tk}) - P_{bb'tk} - (1-u_{bb'tk})M \le 0 \quad \forall l \in \mathcal{L}, t,(b,b') \in l \tag{7c}$$

$$u_{bb'tk}\underline{P}_{bb'} \le P_{bb'tk} \le u_{bb'tk}\overline{P}_{bb'} \quad \forall t,(b,b') \in l, l \in \mathcal{L} \tag{7d}$$

$$B_{bb'}(\theta_{btk} - \theta_{b'tk}) = P_{bb'tk} \quad \forall k, l \in \overline{\mathcal{L}}, t,(b,b') \in l \tag{7e}$$

$$\underline{P}_{bb'} \le P_{bb'tk} \le \overline{P}_{bb'} \quad \forall k, l \in \overline{\mathcal{L}}, t,(b,b') \in l \tag{7f}$$

$$\underline{R}_g \le P_{g(t+1)} - P_{gt} \le \overline{R}_g \quad \forall t,g \tag{7g}$$

$$\underline{P}_g \le P_{gt} \le \overline{P}_g \quad \forall t,g \tag{7h}$$

$$\underline{\theta}_b \le \theta_{btk} \le \overline{\theta}_b \quad \forall t,b,k \tag{7i}$$

where (7b)–(7d) present the constraints that represent the states of lines impacted by the event and the corresponding power flow. All system topologies of possible SSSRs are represented by $u_{bb'tk}$ $\forall t,(b,b') \in l, l \in \mathcal{L}$.

Because there are numerous possible system topologies in consideration of uncertain event influences on a large scale system, the curse of dimensionality leads to difficulty in solving the model. For these numerous possible system topologies, some of system topology scenarios occur with very small probabilities, and ignoring the system topology scenario with a small probability can be used to address the curse of dimensionality. To this end, the system topology scenarios are generated by the Monte Carlo method. To construct the function of the generated system topology scenarios with regard to optimization variables, i.e., on–off states of lines, in the model, a group of additional constraints need to be included. An example is used to explain this. For example, we have three transmission lines l_1, l_2, and l_3 on the sequential trajectory. If we consider all possible system topology scenarios, there will be $2^3 = 8$ topology scenarios. Binary variables x_1, x_2, and x_3, indicating the states of three lines, can be used to represent all topology scenarios. '0' and '1' denote the off-state and the on-state of the lines, respectively. If we only need to include some topology scenarios, e.g., $\{x_1,x_2,x_3\} \in \{\{0,1,1\},\{1,1,1\}\}$, and two new binary variables z_1 and z_2, representing the selection of scenarios, are introduced to include these two topology scenarios in the model. $z_1 = 0, z_2 = 1$ represents that the scenario $\{0,1,1\}$ is selected, and $z_1 = 1, z_2 = 0$ means the scenario $\{1,1,1\}$ is selected. Therefore, the corresponding constraints regarding to the variables x and z are represented as (8).

$$z_1 = x_1x_2x_3 \tag{8a}$$

$$z_2 = (1-x_1)x_2x_3 \tag{8b}$$

$$z_1 + z_2 = 1 \tag{8c}$$

$$z_1,z_2,x_1,x_2,x_3 \in \{1,0\} \tag{8d}$$

where (8a) and (8b) show the relations between line variables and scenario selection variables. (8c) means that only one topology scenario can be chosen.

Eq. (8a) is nonconvex, however, it can be transformed into a set of equivalent inequality constraints by means of recursive McCormick envelopes [47]. Let $\alpha = x_1x_2$, and we have $z_1 = \alpha x_3$ with (8a). With the McCormick envelope method, (8a) can be equivalently rewritten as follows.

$$\alpha \ge x_1 + x_2 - 1, \quad \alpha \le x_1, \quad \alpha \le x_2 \tag{9a}$$

$$z_1 \ge \alpha + x_3 - 1, \quad z_1 \le \alpha, \quad z_1 \le x_3 \tag{9b}$$

Similarly, the multilinear constraints (8b) can be equivalently rewritten as (10) with the new binary variables $\beta = x_2(1-x_1)$.

$$\beta \ge -x_1 + x_2, \quad \beta \le 1 - x_1, \quad \beta \le x_2 \tag{10a}$$

$$z_2 \ge \beta + x_3 - 1, \quad z_2 \le \beta, \quad z_2 \le x_3 \tag{10b}$$

Eqs. (8a)–(8b) show the additional constraints on system topology changes with regard to variables of line states. With (9) and (10), the additional constraints on system topology changes are transformed into mixed integer linear programming. The generic additional constraints on system topology changes with regard to variables of line states can be expressed as follows.

$$z_k = \prod_{t,l\in L,(b,b')\in l} (1-2r_{bb'tk})(1-u_{bb'tk} - r_{bb'tk}) \quad \forall k \tag{11a}$$

$$\sum_k z_k = 1 \tag{11b}$$

$$z_k, u_{bb'tk} \in \{0,1\} \qquad \forall k,t,(b,b') \in \mathcal{L} \tag{11c}$$

where $r_{bb'tk}$ is a given value that represents the corresponding coding state, e.g., "0" and "1" in $\{\{1,1,1\},\{0,1,1\}\}$. z_k denotes the scenario selection variable, and $u_{bb'tk}$ is the line state variable corresponding to x in the example (8). The constraints (11b) and (11c) correspond to (8c) and (8d), and the constraint (11a) corresponds to (8a) and (8b) in the example. In (11a), there exists a generic term $u_1u_2\cdots u_S$, and the subscript S denotes the number of binary variables. By means of the recursive McCormick envelopes, the multilinear term $u_1u_2\cdots u_S$ can be represented as a set of mixed integer linear programming-based constraints. First, the term $u_1u_2\cdots u_S$ is expressed as (12) by introducing binary variables $\zeta_2, \zeta_3, \cdots, \zeta_S$.

$$\begin{aligned} &\zeta_2 = u_1u_2 \\ &\zeta_3 = \zeta_2u_3 \\ &\cdots \\ &\zeta_S = \zeta_{S-1}u_S \end{aligned} \tag{12}$$

where each constraint in (12) is a bilinear constraint, and it can be equivalently transformed into the following constraints.

$$\begin{aligned} &\zeta_2 \geq u_2 + u_1 - 1 \\ &\zeta_2 \leq u_1 \\ &\zeta_2 \geq 0 \\ &\zeta_2 \leq u_2 \\ &\zeta_i \geq u_i + \zeta_{i-1} - 1 \quad (i = 3,\ldots,S) \\ &\zeta_i \leq \zeta_{i-1} \quad (i = 3,\ldots,S) \\ &\zeta_i \geq 0 \quad (i = 3,\ldots,S) \\ &\zeta_i \leq u_i \quad (i = 3,\ldots,S) \end{aligned} \tag{13}$$

where all of the multilinear terms in (11a) can be equivalently transformed into a set of mixed integer linear programming-based constraints. The first four constraints in (13) correspond to $\zeta_2 = u_1u_2$, and the last four generic constraints correspond to $\zeta_i = \zeta_{i-1}u_i$ $(i = 3,\ldots,S)$.

Therefore, the model (7) can be rewritten as a generic expression (14) with the additional constraints (11b), (11c) and (13).

$$\forall \mathcal{U},\ \exists \mathcal{Y}:\ \mathcal{C}\cdot\mathcal{U} + \mathcal{A}\cdot\mathcal{Y} \leq \mathcal{B} \tag{14}$$

where $\mathcal{A}$, $\mathcal{B}$, and $\mathcal{C}$ are the coefficient matrices, where the elements correspond to the constraints (7a)–(7i). $\mathcal{Y}$ is a continuous variable vector, where each element represents operational conditions, and $\mathcal{U}$ is a binary variable vector, in which each element represents the line state.

The constraint (7) indicates that there exist strategies that satisfy the operational constraints for all SSSRs in consideration of the uncertain impacts caused by the event. To this end, we rewrite the model as follows.

$$F(\mathcal{Y}) = \min_{\mathbf{s}^-,\mathbf{s}^+,\mathcal{Y}} \mathbf{1}^T\cdot\mathbf{s}^- + \mathbf{1}^T\cdot\mathbf{s}^+ \tag{15a}$$

$$s.t.\ \ \forall\mathcal{U},\ \ \exists\mathcal{Y},\quad \mathbf{s}^+ - \mathbf{s}^- + \mathcal{C}\cdot\mathcal{U} + \mathcal{A}\cdot\mathcal{Y} \leq \mathcal{B} \tag{15b}$$

$$\mathbf{s}^+ \geq \mathbf{0},\ \mathbf{s}^- \geq \mathbf{0} \tag{15c}$$

where (15) means to find an operational point satisfying the worst-case system topology caused by the event. Equivalently, a max–min optimization model can be employed to rewrite (15).

$$F(\mathcal{Y}) = \max_{\mathcal{U}} \min_{\mathbf{s}^+,\mathbf{s}^-,\mathcal{Y}} \mathbf{1}^T\cdot\mathbf{s}^- + \mathbf{1}^T\cdot\mathbf{s}^+ \tag{16a}$$

$$s.t.\ \ \mathbf{s}^+ - \mathbf{s}^- + \mathcal{C}\cdot\mathcal{U} + \mathcal{A}\cdot\mathcal{Y} \leq \mathcal{B} \tag{16b}$$

$$\mathbf{s}^+ \geq \mathbf{0},\quad \mathbf{s}^- \geq \mathbf{0} \tag{16c}$$

where (16) can be further represented as an optimization model with two levels as (17).

$$F(\mathcal{Y}) = \max_{\mathcal{U}}\ \mathbf{1}^T\cdot(\mathbf{s}^-)^* + \mathbf{1}^T\cdot(\mathbf{s}^+)^* \tag{17a}$$

$$s.t.\ \min_{\mathbf{s}^+,\mathbf{s}^-,\mathcal{Y}}\ \mathbf{1}^T\cdot\mathbf{s}^- + \mathbf{1}^T\cdot\mathbf{s}^+ \tag{17b}$$

$$s.t.\ \ \mathbf{s}^+ - \mathbf{s}^- + \mathcal{C}\cdot\mathcal{U} + \mathcal{A}\cdot\mathcal{Y} \leq \mathcal{B} \tag{17c}$$

$$\mathbf{s}^+ \geq \mathbf{0} \tag{17d}$$

$$\mathbf{s}^- \geq \mathbf{0} \tag{17e}$$

where $(\mathbf{s}^-)^*$ and $(\mathbf{s}^+)^*$ represent the optimal solutions of the lower-level optimization model (17b)–(17d).

3.3. Solution

There is a lower-level optimization model in the constraints of (17), and this results in difficulty in solving the entire optimization model. The lower-level optimization model (17b)–(17e) can be equivalently transformed into a group of inequality/equality constraints with Karush–Kuhn–Tucker (KKT) conditions by introducing Lagrange multiplier vectors α, β and γ with regard to (17c), (17d), and (17e). Eq. (18) lists the corresponding Lagrangian function with regard to (17b)–(17e).

$$\begin{aligned} L_F = {} & \mathbf{1}^T\mathbf{s}^+ + \mathbf{1}^T\mathbf{s}^- + \\ & \alpha^T(\mathcal{C}\cdot\mathcal{U} + \mathcal{A}\cdot\mathcal{Y} + \mathbf{s}^+ - \mathbf{s}^- - \mathcal{B}) - \\ & \gamma^T\mathbf{s}^- - \beta^T\mathbf{s}^+ \end{aligned} \tag{18}$$

With the Lagrangian function, the KKT conditions of the sub-optimization model (17b)–(17e) with regard to $\mathcal{Y}^*$, $(\mathbf{s}^+)^*$, and $(\mathbf{s}^-)^*$ can be represented as follows.

$$\frac{\partial L_F}{\partial \mathbf{s}^-} = \mathbf{1} - \alpha - \gamma = 0 \tag{19a}$$

$$\frac{\partial L_F}{\partial \mathbf{s}^+} = \mathbf{1} + \alpha - \beta = 0 \tag{19b}$$

$$\frac{\partial L_F}{\partial \mathcal{Y}} = \mathcal{A}^T\cdot\alpha = 0 \tag{19c}$$

$$-(\mathbf{s}^+)^* \leq \mathbf{0} \tag{19d}$$

$$-(\mathbf{s}^-)^* \leq \mathbf{0} \tag{19e}$$

$$(\mathbf{s}^+)^* - (\mathbf{s}^-)^* + \mathcal{C}\cdot\mathcal{U} + \mathcal{A}\cdot\mathcal{Y}^* - \mathcal{B} \leq \mathbf{0} \tag{19f}$$

$$\gamma \geq \mathbf{0} \tag{19g}$$

$$\beta \geq \mathbf{0} \tag{19h}$$

$$\alpha \geq \mathbf{0} \tag{19i}$$

$$\hat{\beta}\cdot(\mathbf{s}^+)^* = \mathbf{0} \tag{19j}$$

$$\hat{\gamma}\cdot(\mathbf{s}^-)^* = \mathbf{0} \tag{19k}$$

$$\hat{\alpha}\cdot((\mathbf{s}^+)^* - (\mathbf{s}^-)^* + \mathcal{C}\cdot\mathcal{U} + \mathcal{A}\cdot\mathcal{Y}^* - \mathcal{B}) = 0 \tag{19l}$$

where $\hat{\alpha}$ is a diagonal matrix in which the diagonal element corresponds to the element in the vector α. Similarly, $\hat{\beta}$ and $\hat{\gamma}$ also represent diagonal matrices with regard to β and γ.

With the KKT conditions, the optimization model is reformulated as follows.

$$\max_{\mathcal{U},\mathcal{Y}^*,(\mathbf{s}^+)^*,(\mathbf{s}^-)^*} \mathbf{1}^T\cdot(\mathbf{s}^+)^* + \mathbf{1}^T\cdot(\mathbf{s}^-)^* \tag{20a}$$

$$s.t. \qquad \text{(19c)-(19k)} \tag{20b}$$

where (20) is a mixed integer linear programming-based optimization model. When the optimal value of the model (20) is 0, i.e., $\mathbf{s}^+ = 0$ and $\mathbf{s}^- = 0$, it indicates that an appropriate operational point without load shedding in the sequential time periods is found to satisfy the generated system topology scenarios caused by the event. When $\mathbf{s}^+$ and $\mathbf{s}^-$ are larger than zeros, it indicates that an appropriate operational point without load shedding in the sequential time periods cannot be found to satisfy the generated system topology scenarios caused by the event. $\mathbf{s}^+$ and $\mathbf{s}^-$ are slack variables. When their variables are larger than zeros, the physical meaning is that load shedding at certain buses should be performed to guarantee a feasible operational point

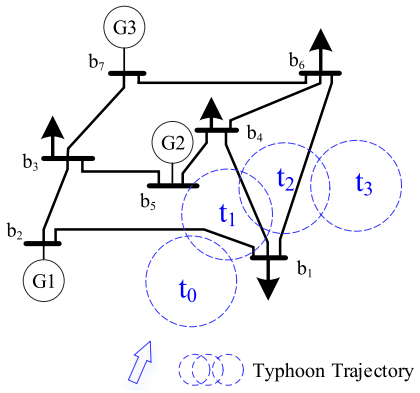

Fig. 5. Sequential impacts caused by a typhoon.

Table 1
Line parameters.

Line No.	To bus	From bus	Line capacity (p.u.)
1	2	1	0.65
2	4	1	0.65
3	6	1	0.65
4	3	2	0.9
5	5	3	0.9
6	5	4	0.8
7	6	4	0.8
8	7	6	0.9
9	7	3	0.9

Table 2
Possible component failure scenarios in t_1 and t_2.

No.	Component failure	
	t_1	t_2
1	–	–
2	–	b_1–b_4
3	–	b_1–b_6
4	–	b_1–b_4, b_1–b_6
5	b_1–b_2	–
6	b_1–b_2	b_1–b_4
7	b_1–b_2	b_1–b_6
8	b_1–b_2	b_1–b_4, b_1–b_6
9	b_1–b_4	–
10	b_1–b_4	b_1–b_6
11	b_1–b_2, b_1–b_4	–
12	b_1–b_2, b_1–b_4	b_1–b_6

Table 3
Line power flow.

No.	Line Power Flow	
	t_1	t_2
1	–	0.5238
2	0.2050	–
3	0.1950	0.1238
4	0.6050	0.2312
5	0.0900	0.0345
6	**0.8000**	0.5255
7	0.0100	0.0745
8	0.7850	0.5507
9	0.1150	0.1343

satisfying the generated system topology scenarios in the sequential time periods. Based on the proposed SSSR-based model, it is easy to find an optimal strategy that improves the system resilience against the extreme weather event.

4. Results and discussions

The proposed SSSR-based model is validated by a simple system and a revised IEEE 118-bus system. In the case studies, typhoons are our focused extreme weather events.

4.1. Case 1: A simple system

The typhoon trajectory and the system topology are presented in Fig. 5. There are three generating units G_1, G_2 and G_3 that are connected to the buses b_2, b_5, and b_7. The upper/lower capacity bounds of each generating unit are 2.5 (p.u.) and 0.2 (p.u.), respectively. Loads connected to the buses b_1, b_3, b_4, and b_6 are 0.4 (p.u.), 0.4 (p.u.), 0.6 (p.u.), and 0.6 (p.u.). The network is directly influenced by the typhoon in t_1 and t_2. Though the typhoon does not directly impact the system in t_0, the operational condition in t_0 has a great impact on the subsequent operational conditions in t_1 and t_2 because of the operational constraints, e.g., possible topology changes due to the typhoon and generators' ramping rates. So, we investigate the optimal strategies in t_0, t_1, and t_2. Table 1 shows the line parameters.

When performing the strategy in t_0, the possible system topology changes in t_1 and t_2 should be taken into account, i.e., uncertain SSSRs should be included. The possible topology changes in t_1 and t_2 are listed in Table 2. When generators' ramping rates are 0.15 (p.u.) and 0.35 (p.u.), the feasible dispatch regions in t_0, in consideration of possible SSSR's impacts of the subsequent time periods t_1 and t_2, are illustrated as blue regions in Fig. 6(a) and (b). Due to the multiple dimensions caused by the sequential steady-state security region over the timeline, we only show the region projection of the sequential steady-state security region on one decision time, e.g., the time t_0.

Take the operational point A as an example, it corresponds to $P_{G_1} = 0.62$, $P_{G_2} = 0.70$, and $P_{G_3} = 0.68$ in t_0. When all of generators' ramping rates are set to 0.15 (p.u.), it is within the feasible dispatch region. Line power flows in consideration of possible failure scenarios in t_1 and t_2 due to the typhoon are presented in Fig. 7(a) and (b). Results show that the line power flows corresponding to all scenarios are within the bounds. Take the operational point B as another example, and this point corresponds to $P_{G_1} = 0.62$, $P_{G_2} = 0.90$, and $P_{G_3} = 0.48$ in t_0. When all of generators' ramping rates are 0.15(p.u.), this point is out of the feasible dispatch region. Table 3 lists the corresponding line power flows with regard to the failure scenario 5. The line power of the line 5-4 reaches the line capacity bound when the optimal strategy, i.e., curtailing 0.015 (p.u.) load at bus b_4 in t_1, is performed. This indicates that we cannot find a feasible operational point satisfying the constraints without load shedding.

For the operational point C, it has the same generators' outputs as the operational point B. When we have the generators' ramping rates as 0.35 (p.u.), the feasible region increases and the operational point C is located in the feasible region. The corresponding line power flows in consideration of all possible system topologies due to the typhoon in t_1 and t_2 are presented in Fig. 8(a) and (b), respectively. Results show that the line power flows corresponding to all scenarios satisfy the bounds. This shows that larger generators' ramping rates lead to a larger sequential steady-state security region.

In addition, different system parameters also impact the optimal operational points over sequential time periods. For example, the ramping rates of the generators are set to 0.15 (p.u.), and the capacity limits of the lines b_4 and b_5 are both set to three scenarios, i.e., 0.7 (p.u.), 0.8 (p.u.), 0.9 (p.u.). Fig. 9 presents the feasible dispatch regions in t_0 with regard to the line capacity limits as 0.7 (p.u.), 0.8 (p.u.), 0.9 (p.u.), respectively, in consideration of the sequential steady-state security region in t_1 and t_2. Similarly, due to the multiple dimensions caused by the sequential steady-state security region over the timeline, we only show the region projection of the sequential steady-state security region on one decision time, e.g., the time t_0. Results show that a larger line capacity bound results in a larger sequential steady-state security

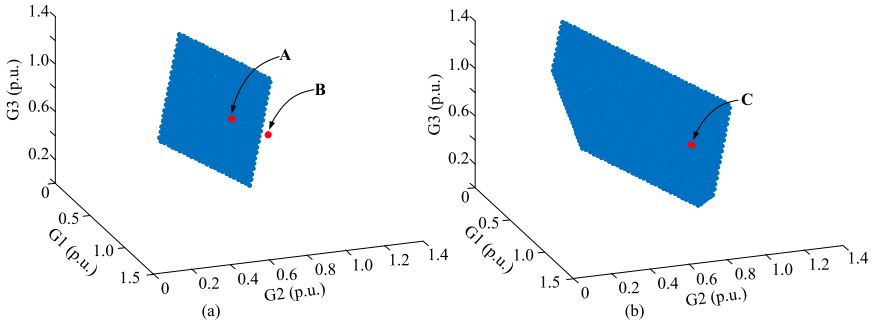

Fig. 6. Region projection of the sequential steady-state security region on t_0 with ramping rates as 0.15 p.u. (a) and 0.35 p.u. (b).

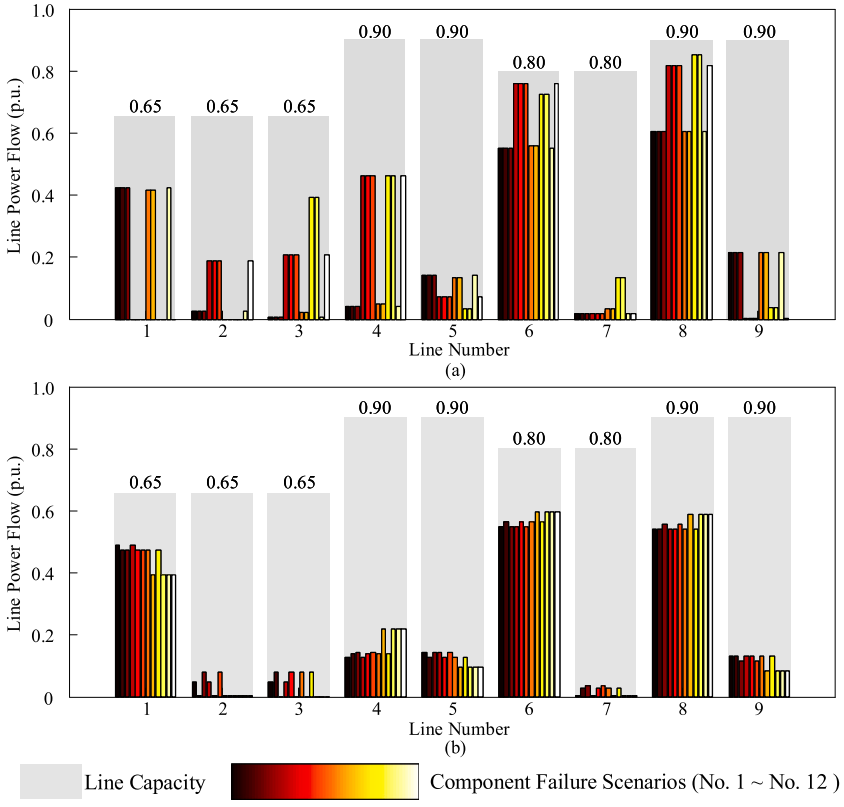

Fig. 7. Power flows under difficult failure scenarios with ramping rate as 0.15 p.u. in t_1 (a) and t_2 (b), respectively.

region. In practice, the system can be dispatched to an operational point located in the sequential steady-state security region in consideration of event's uncertainty on the system.

4.2. Case 2: IEEE 118-bus system

Fig. 10 shows the trajectory of a typhoon and the system topology impacted by the typhoon. It is assumed that all of generators' ramping rates are set to 0.25. For the sake of exposition, the line failure probabilities caused by the typhoon on its trajectory are assumed to 0.05. In practice, the failure probabilities can be calculated based on the existing research studies [45,46].

For this large system, there will exist the curse of dimensionality with regard to possible system topologies on the trajectory of the typhoon in consideration of line failure probabilities. It is not easy to include all possible topologies in the model. Furthermore, some uncertain topologies over the sequential time periods occur with a very low probability so that it could be ignored in the analysis. To this end, the Monte Carlo method is employed to produce the system topology scenarios caused by the typhoon in the analysis. We tested 200, 600, 1000, and 1400 system topology scenarios. Fig. 11(a), (b), (c), and (d) present the optimal operational points in t_0 when having 200, 600, 1000, and 1400 system topology scenarios with the Monte Carlo method, respectively. Results show that the profiles of generator outputs are closer when more system topology scenarios, e.g., 1000 scenarios and 1400 scenarios, are considered. When having more system topology scenarios, the closer profiles also indicate that the SSSR based on generated topology scenarios from the Monte Carlo method could approximate the original SSSR based on all possible topology scenarios. Fig. 12 shows 600 possible line failure scenarios, corresponding to 600 system topology scenarios, during the sequential time periods of the typhoon over the system. The horizontal axis denotes the number of line failure scenarios. The vertical axis denotes the line failure, and different colors mean different lines in failure. With the dispatched generation, Fig. 13 and Fig. 14 show the power flow of 25 lines in t_1 and t_4 under 600 possible system topology scenarios. Different colors show different possible line failure scenarios, i.e., different system topology scenarios. The 25 lines are 5-6, 8-5, 4-11, 23-24, 8-30, 26-30, 23-32, 31-32, 30-38, 41-42, 47-49, 64-61, 64-65, 65-68, 68-69, 17-30,

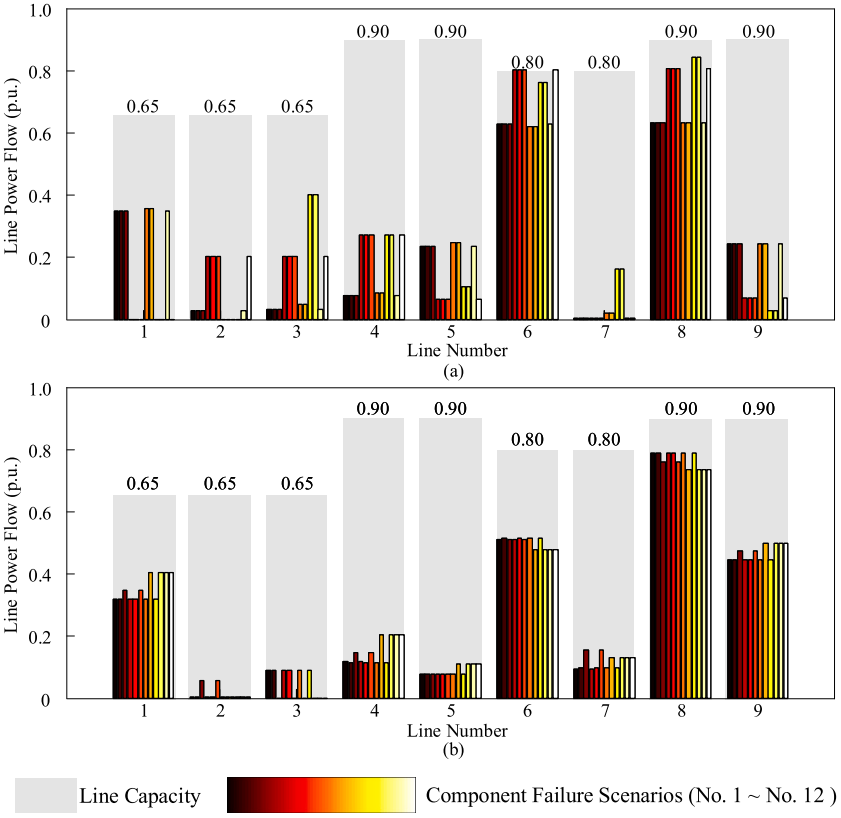

Fig. 8. Power Flow with ramping rate 0.35 p.u. in t_1 (a) and t_2 (b), respectively.

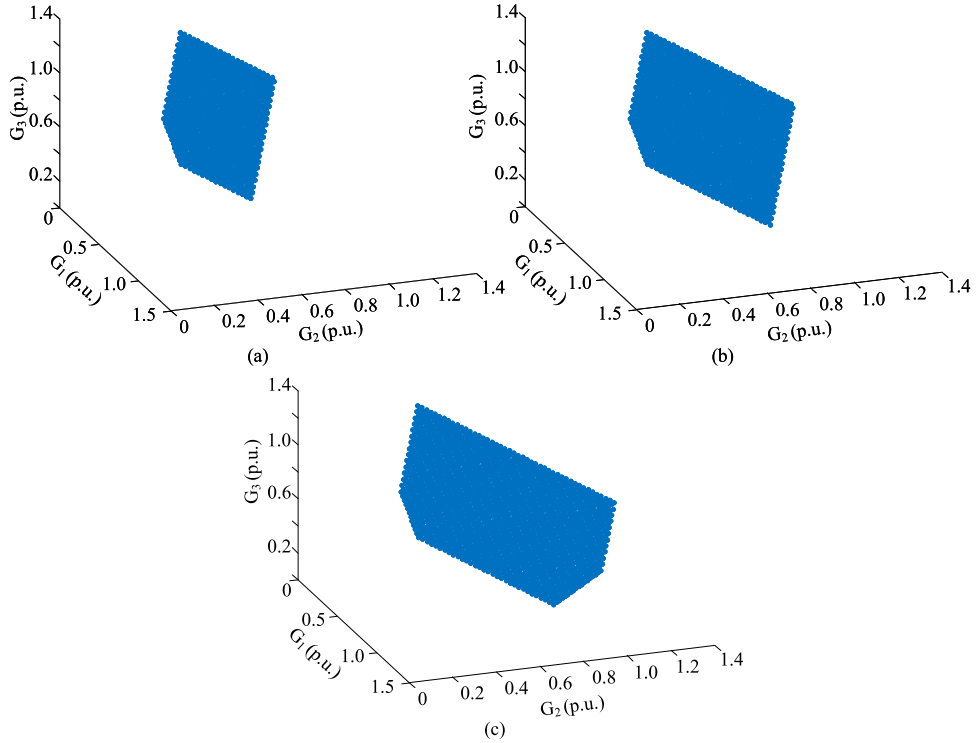

Fig. 9. Region projection of the sequential steady-state security region on t_0 with the line capacities as 0.7 (a), 0.8 (b), 0.9 (c), respectively.

37-38, 49-51, 59-61, 63-59, 69-70, 24-72, 71-72, 74-77, and 75-118, respectively. In practice, topology scenarios in consideration of typhoon information are first generated by means of the Monte Carlo method, and then the system is dispatched to the feasible dispatch region to against the typhoon with the SSSR-based model.

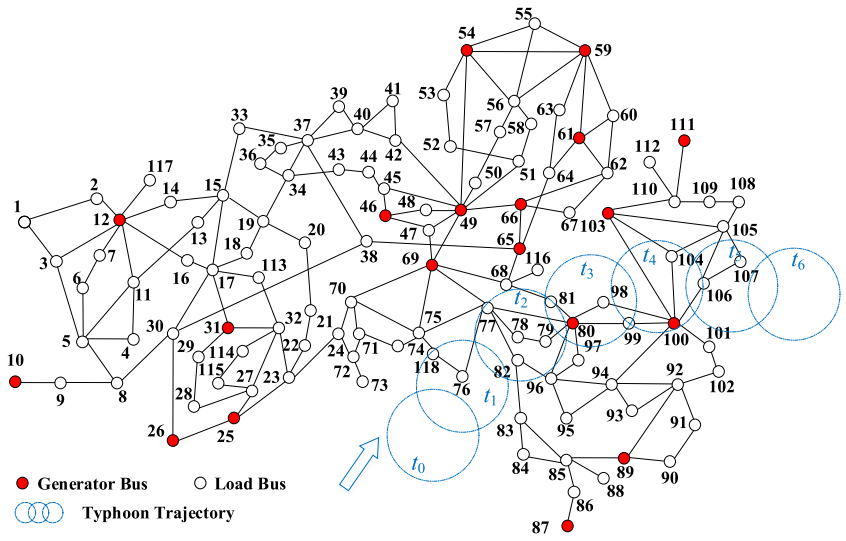

Fig. 10. IEEE 118-bus system topology.

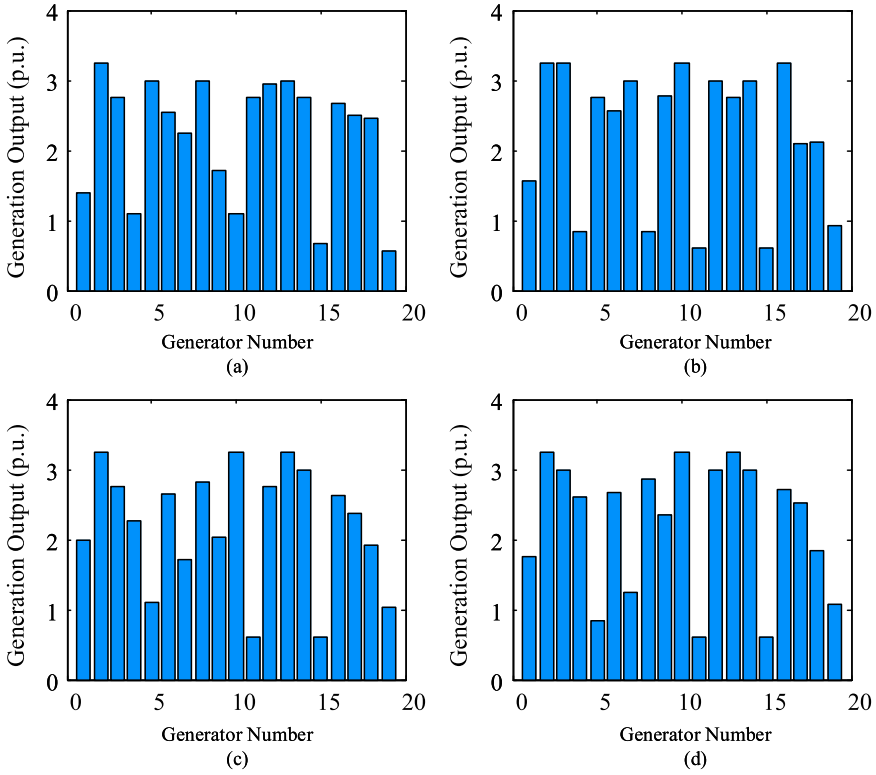

Fig. 11. Generation profiles when having different topology scenarios.

5. Conclusion

To include sequential impacts of an unfolding typhoon, this paper investigates how to consider its uncertain impacts on the system and depict the corresponding feasible region in consideration of sequential impacts with the operational constraints. A sequential steady-state security region (SSSR) is proposed. A SSSR-based bilevel optimization model is established to find an optimal strategy satisfying the operational constraints considering the worst-case topology scenario due to the extreme weather event. In the lower level, the sub-optimization model is equivalently transformed into a set of inequality constraints with the KKT conditions. To address the curse of dimensionality regarding to possible system topologies caused by the typhoons, the Monte Carlo method is employed to produce system topology scenarios with component failure probability due to the extreme weather event, and the recursive McCormick envelopes are used to map the generated topology scenarios to binary variables in the model. The proposed model is validated by two test systems. The first test system concludes that the sequential steady-state security region is impacted by operational bounds, e.g., line thermal capacity limits and generators' ramping rates. The second test system demonstrates the reasonability of SSSR based on the generated system topology scenarios with regard to a larger scale system.

In the future, the following directions on system resilience can be focused on. (1) The first one is multiple energy system resilience. With the development of multiple energy systems, different energy systems

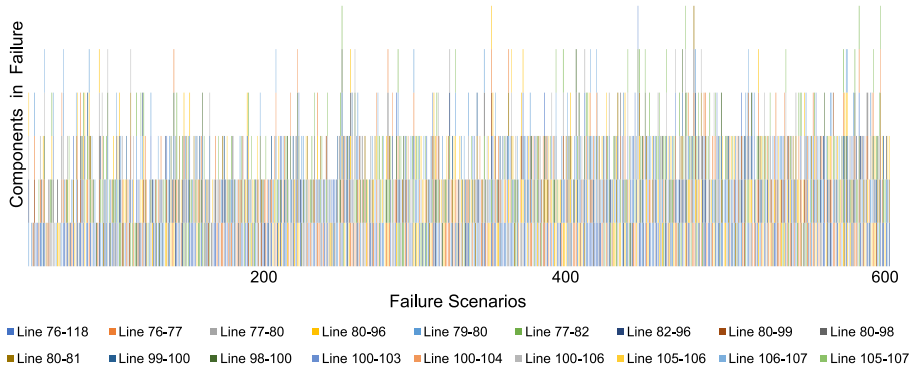

Fig. 12. Line failure scenarios.

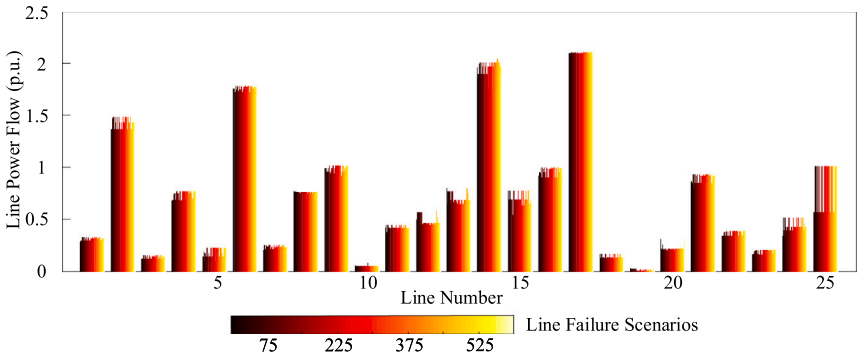

Fig. 13. Line power flow in t_1 with 600 system topology scenarios.

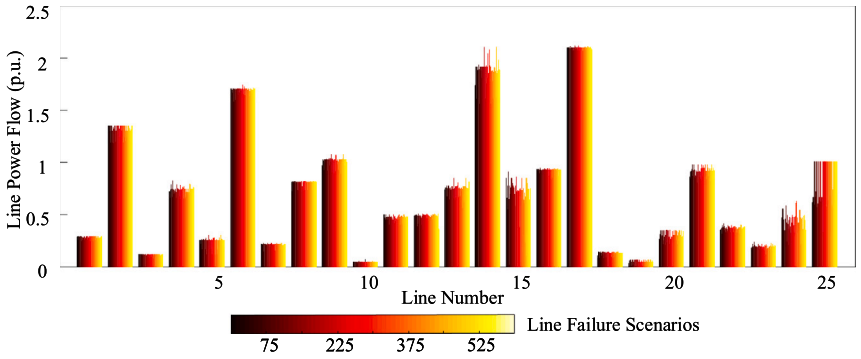

Fig. 14. Line Power Flow in t_4 with 600 system topology scenarios.

have increased couplings that drive them depend on each other. However, different energy systems have different dynamic characteristics with regard to disturbances. For example, power systems have fast dynamic responses to distributions compared to gas systems. When a system is in failure and needs to dispatch repair crews, it is necessary to consider transportation availability, and this response is more slower. How to model these impacts from the perspective of different time scales is one of important tasks. (2) The second one is the impact of stochastic sources on system resilience. When a system is impacted by an extreme weather event, it is more vulnerable compared to that in the normal weather conditions. In this case, the uncertain impacts of stochastic sources on the system cannot be ignored, and it is necessary to have systematic theories to address this issue. (3) The third one is system stability under extreme weather events . Components, e.g., lines, generators, and transformers, may be in failure due to extreme weather events, and in consequence may lead to cascading failures and system instability. Therefore, appropriate strategies need to be implemented to avoid cascading failures and system instability.

CRediT authorship contribution statement

Chong Wang: Conceptualization, Modeling, Methodology, Validation, Writing, Software. **Ping Ju:** Conceptualization, Investigation. **Feng Wu:** Investigation, Methodology. **Shunbo Lei:** Methodology, Validation. **Xueping Pan:** Conceptualization.

Declaration of competing interest

The authors declare that they have no known competing financial interests or personal relationships that could have appeared to influence the work reported in this paper.

Acknowledgments

The authors acknowledge financial supports from the National Natural Science Foundation of China (51907050 and 51837004), the National Key Research and Development Program of China

(2019YFE0105200), and the Fundamental Research Funds for the Central Universities, China (B200202169).

References

[1] Abdin IF, Fang YP, Zio E. A modeling and optimization framework for power systems design with operational flexibility and resilience against extreme heat waves and drought events. Renew Sustain Energy Rev 2019;112:706–19.

[2] Mishra DK, Ghadi MJ, Azizivahed A, Li L, Zhang J. A review on resilience studies in active distribution systems. Renew Sustain Energy Rev 2021;135:110201.

[3] Wang Y, Rousis AO, Strbac G. On microgrids and resilience: A comprehensive review on modeling and operational strategies. Renew Sustain Energy Rev 2020;134:110313.

[4] Martin N, Rice J. Power outages, climate events and renewable energy: Reviewing energy storage policy and regulatory options for Australia. Renew Sustain Energy Rev 2021;137:110617.

[5] Molyneaux L, Brown C, Wagner L, Foster J. Measuring resilience in energy systems: Insights from a range of disciplines. Renew Sustain Energy Rev 2016;59:1068–79.

[6] Mukherjee S, Nateghi R, Hastak M. A multi-hazard approach to assess severe weather-induced major power outage risks in the U.S.. Reliab Eng Syst Saf 2018;175:283–305.

[7] Wanik DW, Anagnostou EN, Astitha M, Hartman BM, Lackmann GM, Yang J, Cerrai D, He J, Frediani MEB. A case study on power outage impacts from future hurricane sandy scenarios. J Appl Meteorol Climatol 2018;57(1):51–79.

[8] Alhelou HH, Hamedani-Golshan ME, Njenda TC, Siano P. A survey on power system blackout and cascading events: Research motivations and challenges. Energies 2019;12:682.

[9] Douglas E, Mcgee K, Mccullough J. Texas leaders failed to heed warnings that left the state's power grid vulnerable to winter extremes. URL https://www.texastribune.org/2021/02/17/texas-power-grid-failures/.

[10] USDepartment of Energy. State of Texas: Energy sector risk profile. URL https://www.energy.gov/sites/prod/files/2016/09/f33/TX_Energy.

[11] Electric Reliability Council of Texas. ERCOT Quick Facts for 2017. URL http://www.ercot.com/content/wcm/lists/144926/ERCOT_Quick_Facts_72418.pdf.

[12] Ahmadi S, Saboohi Y, Vakili A. Frameworks, quantitative indicators, characters, and modeling approaches to analysis of energy system resilience: A review. Renew Sustain Energy Rev 2021;144:110988.

[13] Andoni M, Robu V, Flynn D, Abram S, Geach D, Jenkins D, McCallum P, Peacock A. Blockchain technology in the energy sector: A systematic review of challenges and opportunities. Renew Sustain Energy Rev 2019;100:143–74.

[14] Cristiano S, Ulgiati S, Gonella F. Systemic sustainability and resilience assessment of health systems, addressing global societal priorities: Learnings from a top nonprofit hospital in a bioclimatic building in Africa. Renew Sustain Energy Rev 2021;141:110765.

[15] Severe impact resilience: consideration and recommendation. Tech. rep., North American Electric Reliability Corporation; 2012.

[16] Das L, Munikoti S, Natarajan B, Srinivasan B. Measuring smart grid resilience: Methods, challenges and opportunities. Renew Sustain Energy Rev 2020;130:109918.

[17] Emenike SN, Falcone G. A review on energy supply chain resilience through optimization. Renew Sustain Energy Rev 2020;134:110088.

[18] Tari AN, Sepasian MS, Kenari MT. Resilience assessment and improvement of distribution networks against extreme weather events. Int J Electr Power Energy Systs 2021;125:106414.

[19] Sharifi A, Yamagata Y. Principles and criteria for assessing urban energy resilience: A literature review. Renew Sustain Energy Rev 2016;60:1654–77.

[20] Liu X, Hou K, Jia H, Zhao J, Mili L, Mu Y, Rim J, Lei Y. A resilience assessment approach for power system from perspectives of system and component levels. Int J Electr Power Energy Systs 2020;118:105837.

[21] Shi Q, Li F, Olama M, Dong J, Xue Y, Starke M, Winstead C, Kuruganti T. Network reconfiguration and distributed energy resource scheduling for improved distribution system resilience. Int J Electr Power Energy Systs 2021;124:106355.

[22] Amirioun M, Aminifar F, Lesani H, Shahidehpour M. Metrics and quantitative framework for assessing microgrid resilience against windstorms. Int J Electr Power Energy Systs 2019;104:716–23.

[23] Nateghi R, Guikema S, Quiring S. Forecasting hurricane-induced power outage durations. Nat Hazards 2014;74(3):1795–811.

[24] Trakas DN, Hatziargyriou ND. Optimal distribution system operation for enhancing resilience against wildfires. IEEE Trans Power Syst 2018;33(2):2260–71.

[25] Amirioun MH, Aminifar F, Lesani H. Towards proactive scheduling of microgrids against extreme floods. IEEE Trans Smart Grid 2018;9(4):3900–2.

[26] Bessani M, Massignan JAD, Fanucchi RZ, Camillo MHM, London JBA, Delbem ACB, Maciel CD. Probabilistic assessment of power distribution systems resilience under extreme weather. IEEE Syst J 2019;13(2):1747–56.

[27] Zhang G, Zhang F, Zhang X, Wu Q, Meng K. A multi-disaster-scenario distributionally robust planning model for enhancing the resilience of distribution systems. Int J Electr Power Energy Systs 2020;122:106161.

[28] Cai S, Xie Y, Wu Q, Xiang Z. Robust MPC-based microgrid scheduling for resilience enhancement of distribution system. Int J Electr Power Energy Systs 2020;121:106068.

[29] Arab A, Khodaei A, Khator SK, Ding K, Emesih VA, Han Z. Stochastic pre-hurricane restoration planning for electric power systems infrastructure. IEEE Trans Smart Grid 2015;6(2):1046–54.

[30] Amirioun MH, Aminifar F, Lesani H. Resilience-oriented proactive management of microgrids against windstorms. IEEE Trans Power Syst 2018;33(4):4275–84.

[31] Ma S, Chen B, Wang Z. Resilience enhancement strategy for distribution systems under extreme weather events. IEEE Trans Smart Grid 2018;9(2):1442–51.

[32] Lei S, Chen C, Zhou H, Hou Y. Routing and scheduling of mobile power sources for distribution system resilience enhancement. IEEE Trans Smart Grid 2019;10(5):5650–62.

[33] Amirioun MH, Aminifar F, Shahidehpour M. Resilience-promoting proactive scheduling against hurricanes in multiple energy carrier microgrids. IEEE Trans Power Systems 2019;34(3):2160–8.

[34] Wang Z, Wang J. Self-healing resilient distribution systems based on sectionalization into microgrids. IEEE Trans Power Syst 2015;30(6):3139–49.

[35] Panteli M, Trakas DN, Mancarella P, Hatziargyriou ND. Boosting the power grid resilience to extreme weather events using defensive islanding. IEEE Trans Smart Grid 2016;7(6):2913–22.

[36] Huang G, Wang J, Chen C, Qi J, Guo C. Integration of preventive and emergency responses for power grid resilience enhancement. IEEE Trans Power Syst 2017;32(6):4451–63.

[37] Wang Y, Huang L, Shahidehpour M, Lai LL, Yuan H, Xu FY. Resilience-constrained hourly unit commitment in electricity grids. IEEE Trans Power Syst 2018;33(5):5604–14.

[38] Wang C, Hou Y, Qiu F, Lei S, Liu K. Resilience enhancement with sequentially proactive operation strategies. IEEE Trans Power Syst 2017;32(4):2847–57.

[39] Wang C, Ju P, Lei S, Wang Z, Wu F, Hou Y. Markov decision process-based resilience enhancement for distribution systems: An approximate dynamic programming approach. IEEE Trans Smart Grid 2020;11(3):2498–510.

[40] Wang Z, Shen C, Xu Y, Liu F, Wu X, Liu C. Risk-limiting load restoration for resilience enhancement with intermittent energy resources. IEEE Trans Smart Grid 2019;10(3):2507–22.

[41] Chen C, Wang J, Qiu F, Zhao D. Resilient distribution system by microgrids formation after natural disasters. IEEE Trans Smart Grid 2016;7(2):958–66.

[42] Jamborsalamati P, Hossain MJ, Taghizadeh S, Konstantinou G, Manbachi M, Dehghanian P. Enhancing power grid resilience through an IEC61850-based EV-assisted load restoration. IEEE Trans Industrial Informatics 2020;16(3):1799–810.

[43] Lei S, Chen C, Li Y, Hou Y. Resilient disaster recovery logistics of distribution systems: Co-optimize service restoration with repair crew and mobile power source dispatch. IEEE Trans Smart Grid 2019;10(6):6187–202.

[44] Wu F, Kumagai S. Steady-state security regions of power systems. IEEE Trans Circuits Syst 1982;29(11):703–11.

[45] Liu L, Padilla L, Creem-Regehr SH, House DH. Visualizing uncertain tropical cyclone predictions using representative samples from ensembles of forecast tracks. IEEE Trans Vis Comput Graphics 2019;25(1):882–91.

[46] Elsner JB, Jagger TH. A hierarchical Bayesian approach to seasonal hurricane modeling. J Clim 2004;17:2813–27.

[47] Castro PM. Tightening piecewise McCormick relaxations for bilinear problems. Comput Chem Eng 2015;72(2):300–11.